environments

MDPI

Article

Limestone Processing Sludge: From Waste to Sustainable Resource

Mafalda Guedes [1,2], Joana Carrasqueira [3], Tomás Seixas [2], Clélia Afonso [3], Maria Manuel Gil [3,4], Raul Bernardino [3,5,6], Roberto Gamboa [3] and Susana Bernardino [3,5,6,*]

1 UnIRE, Department of Mechanical Engineering, Instituto Superior de Engenharia de Lisboa, Instituto Politécnico de Lisboa, Rua Conselheiro Emídio Navarro 1, 1959-007 Lisboa, Portugal; mafalda.guedes@isel.pt
2 CeFEMA-LaPMET, Instituto Superior Técnico, Universidade de Lisboa, Av. Rovisco Pais 1, 1049-001 Lisboa, Portugal; tomas.seixas@tecnico.ulisboa.pt
3 MARE—Marine and Environmental Sciences Centre, ARNET—Aquatic Research Network, School of Tourism and Maritime Technology, Polytechnic Institute of Leiria, 2520-614 Peniche, Portugal; joana.p.carrasqueira@ipleiria.pt (J.C.); clelia@ipleiria.pt (C.A.); maria.m.gil@ipleiria.pt (M.M.G.); raul.bernardino@ipleiria.pt (R.B.); roberto.gamboa@ipleiria.pt (R.G.)
4 +ATLANTIC—Associação para um Laboratório Colaborativo do Atlântico, Rua do Conhecimento 4, 2520-614 Peniche, Portugal
5 LSRE-LCM—Laboratory of Separation and Reaction Engineering-Laboratory of Catalysis and Materials, School of Tourism and Maritime Technology, Polytechnic Institute of Leiria, 2520-614 Peniche, Portugal
6 ALiCE—Associate Laboratory in Chemical Engineering, Faculty of Engineering, University of Porto, Rua Dr. Roberto Frias, 4200-465 Porto, Portugal
* Correspondence: susana.bernardino@ipleiria.pt

Abstract

The limestone quarrying and processing industry generates huge amounts of waste, with limestone sludge being one of the most prevalent and challenging by-products. This study aims to evaluate the potential of limestone sludge as a sustainable secondary raw material for the mechanochemical synthesis of bioceramics, specifically hydroxyapatite (HA), for high-added-value applications in bone tissue engineering. High-energy milling is innovatively used as the processing route: dry sludge (functioning as the calcium source), a phosphate source, and water were milled with the aim of producing calcium phosphates (in particular, hydroxyapatite) via mechanosynthesis. The industrial sludge was thoroughly analyzed for chemical composition, heavy metals, and mineral phases to ensure suitability for biomedical applications. The mixture of reagents was tailored to comply with Ca/P = 1.67 molar ratio. Milling was carried out at room temperature; the milling velocity was 600 rpm, and milling time ranged from 5 to 650 min. Characterization by XRD, Raman spectroscopy, and SEM confirmed the progressive transformation of calcite into hydroxyapatite through a metastable DCPD intermediate, following logarithmic reaction kinetics. The resulting powders are fine, homogeneous, and phase-pure, demonstrating that mechanosynthesis provides a low-cost and environmentally friendly pathway to convert limestone waste into functional bioceramic materials. This suggests that Moleanos sludge is a viable and sustainable source to produce tailored calcium phosphates and confirms mechanosynthesis as a cost-effective and reliable technology to activate the low-kinetics chemical reactions in the $CaCO_3$-H_3PO_4–H_2O system. This work highlights a novel circular economy approach for the valorization of industrial limestone sludge, turning a difficult waste stream into a high-value, sustainable resource.

Keywords: stone processing residues; limestone sludge; mechanical milling; calcium phosphates; hydroxyapatite; mechanosynthesis

Academic Editor: Ching-Yuan Chang

Received: 2 October 2025
Revised: 17 October 2025
Accepted: 26 October 2025
Published: 30 October 2025

Citation: Guedes, M.; Carrasqueira, J.; Seixas, T.; Afonso, C.; Gil, M.M.; Bernardino, R.; Gamboa, R.; Bernardino, S. Limestone Processing Sludge: From Waste to Sustainable Resource. *Environments* **2025**, *12*, 405. https://doi.org/10.3390/environments12110405

1. Introduction

Limestone is a versatile natural material, abundantly used in a range of industrial sectors [1,2]. Its main application concerns the construction and building industry, where it is used as dimension stone or (mostly) in crushed form—as limestone sand, coarse aggregate, and filler in concrete and roadstone—and as a major component of clinker raw meal in the manufacture of Portland cement [3]. Other uses include agriculture (to raise the pH of acid soils, added to fertilizers and animal foodstuff), metallurgy (fluxing agent in steelmaking and metal smelting), glass-making (fluxing agent), and in quicklime production [3,4]. This results in a global limestone market estimated at USD 79.18 billion in 2024, while a compound annual growth rate (CAGR) of 7.4% between 2025 and 2030 is anticipated [5]. Beyond traditional applications in cement and ceramics, recent research has explored the valorization of limestone and marble sludge in several bioproduct-oriented fields. For instance, calcareous residues have been used as calcium sources in microbially induced calcite precipitation (MICP) for soil improvement and biocementation, as neutralizing agents and nutrient supplements in biofertilizers and agricultural amendments, and as biosorbents for metal or phosphate removal from wastewater due to their high surface reactivity. These examples demonstrate the potential of limestone sludge as a reactive and biocompatible material. However, its direct transformation into high-value bioceramics via mechanochemical synthesis, as proposed in the present study, remains largely unexplored.

Limestone processing involves repeated cutting and sawing and several grinding, polishing, and finishing steps [3]. These operations produce a fine waste fraction overall known as limestone sludge, which includes slurry resulting from the mixing of water, microfine dust, and residual sludge generated during the processing operations [3]. The waste generated from calcareous stone cutting and processing can reach more than 70% of the stone product [6], an amount unlike that of any other extractive industry [3,7]. On average, sludge represents 22.5% of the processed raw material, with a solids fraction less than 10 wt% [6]. It is the most difficult and challenging waste fraction to recover. On the one hand, removing the high moisture content (usually to below 2 wt% H_2O) is critically required by most transformation processes [4,8,9]. In addition to the fact that drying it to such an extent is an energy-intensive and costly operation, the resulting fine particles are subject to handling, storage, and transportation issues, requiring stabilization or pelletization [4,8,9]. On the other hand, sludge composition is inconsistent: depending on the source quarry, it may contain calcite and/or aragonite polymorph (with $CaCO_3$ varying between 90 and 98 wt%); dolomite ($CaMg(CO_3)_2$) $\leq$ 2 wt%, clastic sediments (quartz, clay) $\leq$ 5–10%, and organic matter (~0.2–1%) are frequently present [10–12]. Furthermore, the market value of limestone is low, and the cost of dewatering, drying, loading, and transporting limestone sludge far exceeds the cost of the raw material [8,13]. This seriously limits application even if the sludge is technically acceptable [8,13]. For this reason, its reuse rate is very low, and limestone sludge is mostly disposed of in landfills or used to fill decommissioned quarries [3]. The widespread environmental disturbance caused is incompatible with the increasing and pressing need for environmental care and sustainability [6,14]; thus, achieving an acceptable solution with commercial value is crucial to the value chain of the calcareous stone industry [3,15]. The obligation to reduce the use of nonrenewable natural resources and to minimize the negative environmental impact of quarrying and processing has been fostering increasing interest in sludge recovery and recycling [6]. The use of calcareous sludge is consolidated in the cement and concrete industry (essentially in the same applications as the primary material, either incorporated as filler in cement, as aggregates substitute in concrete, and in clinker production) [3,4]. To a much lesser extent, it is also used in pH correction of acidic agricultural soils [3,4], water treatment of mine drainage, neutralization of acidic water, and precipitation of heavy metals [16,17]. Limestone sludge

is also used, although in a limited and context-dependent fashion, in the traditional ceramics industry [18–21] and in two niche applications: heritage restoration [22] and carbon capture by mineralization [23]. Nevertheless, actual recycling of limestone sludge is very limited, and the largest portion ends up in landfills, unexploited [3,6,7,14]. Thus, there is a crucial need for more sustainable approaches for limestone sludge repurposing and recycling [8,20].

Limestone sludge is characterized by high calcium concentration (34–40 wt% depending on limestone purity) [20], relatively small particle size (from nanometric to approx. 20 μm depending on the quarry source) [3,6,24], high specific surface area, and high reactivity [6]. This is a combination of properties hugely demanded in engineering ceramics, and it is in this context that the current work proposes a novel approach for the recycling of limestone sludge into high-added-value advanced bioceramics. This is expected to offset secondary processing costs while innovating in the production of sustainable materials. In the envisioned application, limestone waste functions as Ca^{2+} source for the mechanosynthesis of calcium phosphate (CaP) bioceramics—e.g., hydroxyapatite (HA), monocalcium phosphate anhydrous (MCPA), and dicalcium phosphate dihydrate (DCPD). The strong interest in the synthesis of CaP, in particular HA, comes from its medical relevance [24–28]: synthetic calcium phosphates are chemical and structurally similar to the mineral phase of human bone and teeth and can be used in bone tissue engineering as bone graft, implant coating, bone cement, and scaffold material [24–28]. Calcium phosphates are also valuable beyond the medical field: because of their ion exchange capacity, adsorption behavior, thermal stability, and chemical versatility they have industrial, environmental, agricultural, and chemical applications [29,30]. These include application in heavy metal removal from wastewater [31], for catalysis [32,33], as membranes and adsorbents [34], and as additives in foodstuff and in advanced food packaging [29,35].

In this work, calcium phosphates are produced via mechanochemical processing of limestone powder obtained after drying sludge. A tailored mixture of dry powder (functioning as calcium source), H_3PO_4 (phosphate source), and H_2O are submitted to high-energy milling during variable milling time to produce calcium phosphate(s) (1).

$$Ca^{2+} + \text{phosphate ion} \longrightarrow \text{calcium phosphate} \quad (1)$$

The used formulation, Ca/P = 1.67 molar ratio, is expected to trigger mechanochemical reactions towards the formation of hydroxyapatite (mechanosynthesis). Mechanosynthesis is a reproducible and straightforward approach to CaP processing when carried out at room temperature [36,37]. Mechanochemical reactions are promoted by the energy transferred from the milling media to the reagents on impact, enabling fragmentation—with creation of fresh surfaces, new active sites and defects, and intimate mixing [38,39]. Overall, it results in significant reactivity increase [38,39], crucial to surpass the well-known kinetic issues in the $CaCO_3$-H_3PO_4-H_2O system, e.g., [40–42].

To the best of the authors knowledge, the current work is the first concerning the use of limestone sludge as reagent in the mechanosynthesis of calcium phosphates, although several reports in the literature concern the wet synthesis route, e.g., [43–45]. Only very few studies [46–49] consider the use of limestone sludge as raw material for bioceramics production. Yet, described results suggest that the synthesized HA can be used as biomedical material, since in vitro biocompatibility assessment showed usual osteoblast cell proliferation, viability, and adhesion properties [49].

An estimated 346,500 sludge tons/year result from stone processing operations in Europe alone [47]. This poses a massive environmental challenge but also makes limestone sludge a highly available material. Leveraging it as a secondary calcium source in the production of synthetic calcium phosphates offers a sustainable and cost-effective

alternative to the primary $CaCO_3$ material. Provided that critical specifications, such as chemical purity, phase consistency, regulatory compliance, and process reproducibility, are rigorously fulfilled, the produced calcium phosphates can pose an alternative to the rapidly expanding global market of bioceramics [46–49]. In this context, the current work envisions the use of limestone sludge as a secondary raw material to be mechanochemically recycled into bioceramics with high added value.

2. Materials and Methods

Although SI units are used throughout this work, some non-SI units (e.g., cm^{-1} for Raman wavenumbers and °C for temperature) are retained, as they are standard in spectroscopy and thermal analysis reporting, ensuring consistency with established material characterization conventions.

2.1. Materials

MARFILPE (Batalha, Portugal) graciously provided sludge resulting from the processing operations of *Moleanos* limestone quarried in the region. *Moleanos* is a whitish-brown limestone (apparent density, 2.570 g/cm^3; max. 0.75% impurities according to supplier). For adequate sampling, ten random aliquots were collected from each sludge container provided by MARFILIPE, mixed, and thoroughly homogenized. The sludge was dried at room temperature until a compact solid agglomerate was obtained. After being deagglomerated, the obtained loose powder was used as calcium source in all further experiments. A commercial H_3PO_4 aqueous solution (85 wt%, Panreac (ITW, Barcelona, Spain) was used as phosphate source; deionized water was used throughout.

2.2. Methods

2.2.1. Moisture Content in the Sludge

The moisture content in the limestone sludge was determined according to ISO 638:2008 specification [50]. The initial sample weight (w_0) was measured, and the sample was dried in oven (Binder FD 23, Binder GmbH, Tuttlingen, Germany) at 105 °C until reaching constant weight (w_f). The moisture content (MC) was calculated according to (2). This procedure was carried out in triplicate for reproducibility assessment.

$$H(\%) = \frac{w_0 - w_f}{w_0} \times 100 \quad (2)$$

This step was essential to determine the residual water content of the sludge, since moisture directly affects powder handling and the reproducibility of the subsequent mechanochemical reactions. The obtained moisture data were used to adjust the Ca/P ratio and the amount of water added during milling.

2.2.2. Characterization of Starting Dry Sludge Particles and Milled Powders

The dry limestone powder was characterized regarding the presence of heavy metals and other metal contaminants using inductively coupled plasma optical emission spectroscopy (ICP-OES) (iCAP 7000, ThermoFisher Scientific, Bremen, Germany)). Nitric acid (>65%, PanReac) and hydrochloric acid (37%, VWR) were mixed in 1:3 molar ratio to prepare aqua regia which was used to digest the sludge samples. Analysis took place under argon, using the following plasma conditions: camera temperature, °C; optics temperature, 38 °C; pump rate, 50 rpm; auxiliary gas flow, 0.5 L/min; nebulizing gas flow, 0.7 L/min. Quantification of Al, P, S, and Fe was carried out by comparison with a calibration curve, built using standards with known concentration. This evaluation was carried out twice upon two different sludges collected by the supplier approx. 1 year apart.

Dry limestone was analyzed by simultaneous differential scanning calorimetry/thermogravimetry (DSC/TG, Hitachi STA200) to assess the presence of organics, loss of water, and loss of CO_2. The powder was placed in an alumina pan and heated up to 1000 °C at 10 °C/min under nitrogen gas flow of 100 mL/min; cooling took place in air. Three samples (9.1 ± 0.1 mg) were tested for reproducibility. Linear background removal was carried out using the Fityk 0.9.8 software [51]; peak onset was identified using the first derivative method.

The starting limestone powder and the produced milled powders were characterized regarding particles' morphology, crystalline phases present, and overall phase composition. The powders were observed by scanning electron microscopy (SEM, Phenom ProX, Thermo Scientific, Whaltam, MA, USA) for microstructural characterization. Samples for SEM observation were previously coated with Au-Pd alloy to prevent charge accumulation during observation. Elemental microanalysis was accomplished using the energy-dispersive X-ray spectroscopy (EDS) system integrated in the equipment. To avoid inaccuracy in quantification arising from the presence of external elements introduced by the coating alloy, samples aimed for EDS were not coated. Particle size distribution of at least five SEM image fields of each powder was determined by image analysis (Image J version 1.52q freeware [52]).

Micro-Raman confocal spectroscopy (HR Evolution, Horiba Jobin-Yvon, Oberusel, Germany) was used to identify the phases present in the starting material, CaP phases formed by mechanosynthesis, and other phases otherwise present. Spectra were collected in the 100–1200 cm^{-1} wavenumber range, with 5 accumulations and acquisition time of 10 s, using a 532 nm laser, 100x objective lens, 200 hole, and 600 grooves/mm grating. Fityk (version 1.3.1) software was used for linear background removal, and peak fitting was carried out with Lorentzian function.

The crystalline phases present in the powders were assessed by X-ray diffraction (XRD) (D8 Advance with SSD160 multichannel detector, Bruker, Billerica, USA). Acquisition was carried out in the 2θ range 10–80° using CuK_α radiation, step size of 0.03°, and step time of 0.5 s; the limit of detection (LOD) indicated by the supplier is between 1 and 2 wt% [53]. A beam knife component was mounted to reduce background scattering at low 2θ angles. Crystalline phase identification was carried out using Match! software, by comparison with diffraction files in the COD database. Raw diffraction data were refined by the Rietveld method using PROFEX (version 5.5.2) software [54]. The refinements were analyzed by comparing the common reliability factors and the difference between experimental and refined curve [55]. The diffractograms presented in Section 3 were afterwards normalized to the most intense peak for comparison purposes.

These analyses ensured that the starting material met the purity and compositional requirements for its use as a calcium precursor in the mechanochemical synthesis of hydroxyapatite.

2.2.3. Mechanosynthesis

The composition of the reagents' mixture and selection of milling conditions were based on the authors' previous experience [36,37]. Each batch contained amounts of limestone powder and H_3PO_4 complying with the Ca/P = 1.67 molar ratio of stoichiometric hydroxyapatite; 50 wt% H_2O (based on dry powder weight) was added. Materials handling prior to milling vial sealing was carried out under NPT conditions for all batches. High-energy mechanical milling took place in a planetary ball mill (Retsch, PM100). Stainless steel vial (250 mL) and balls (6 balls, Æ 10 mm) were used, both from Retsch (maximum impurities < 0.24 wt% according to supplier). The mass of the mixtures in each batch complied with 20:1 ball-to-powder mass ratio. Milling was always carried out at 600 rpm

for time periods ranging from 0.5 to 11 h. The suspensions obtained after milling cycle were oven dried at 60 °C for 24 h and characterized (Section 2.2.2).

The chosen formulation and milling parameters were optimized, based on previous experience, to promote the formation of calcium phosphates under ambient conditions, enabling direct comparison of the effect of milling time on phase evolution.

3. Results

3.1. Sludge Characterization

The gravimetric assay rendered 24.72 ± 0.36 wt% solids load in the supplied sludge, in good agreement with values expected for sludges dewatered by filter-pressing (around 80 wt%) [56].

Table 1 displays the concentration of heavy metals (Hg, Cd, Fe) and other hazardous elements (Al, S) measured by ICP-OES in two samples collected one year apart. The concentration of each species differs greatly, from a minimum of 1.2-fold for iron to a maximum of 10.5-fold for cadmium.

Table 1. ICP-OES elemental composition of sludge particles collected one year apart.

	Concentration	
	Sample 1 (mg/g)	**Sample 2 (mg/g)**
Aluminum	0.0877 ± 0.0027	0.0314 ± 0.0003
Sulfur	1.0928 ± 0.0588	3.582 ± 0.0260
Mercury	<0.0014	<0.00059
Cadmium	<0.0004	<0.00042
Iron	0.1865 ± 0.0306	0.233 ± 0.0007

These results confirm that the sludge composition remains chemically stable over time, with metal concentrations well below regulatory limits, supporting its suitability as a safe calcium source for bioceramic synthesis.

3.2. Powder Particles Characterization After Drying

3.2.1. Particle Morphology

As-dried powder particles (Figure 1a) are micrometric irregular spheres, with a median particle size (d_{50}) around 1132 nm. The associated standard deviation value is high, which was to be expected considering the variety of processing tools and operations that produced the particles [3]. This will be further discussed in § 3.3.1. Dry particles form apparently strong agglomerates (Figure 1b) with a maximum measured size around 18 µm. Micrometric particles with Si/O molar ratio around 0.5 (Figure 1c) and platelets with Ca/O molar ratio around 0.5 (Figure 1d) were also identified by EDS microanalysis and assigned to SiO_2 and $Ca(OH)_2$, respectively.

The X-ray maps in Figure 2 show the spatially resolved elemental distribution in a sample of dry sludge particles. Again, the SEM image (Figure 2a) shows agglomerated fine particles, typical of dried suspensions [57]. Calcium (Figure 2b) is abundant and widespread in the sample, which is consistent with Ca-rich mineral residues in the sludge. This confirms the abundant presence of calcite, the dominant mineral in the quarry; it is also consistent with the presence of $Ca(OH)_2$. Carbon is present throughout the microscopic field (Figure 2c), often correlating with calcium. Its presence is expectedly due to the CO_3^{2-} group of calcite. Oxygen is also present throughout (Figure 2d), supporting the presence of several oxygen-containing anions in the system: CO_3^{2-}, OH^-, PO_4^{3-}, SiO_4^{4-}. The localized bright regions with no special correlation to the other elements were assigned to a

phosphorous-containing phase (Figure 2e). Finally, silicon's presence is sparse but distinct (Figure 2f), suggesting SiO_2-rich domains in the sample.

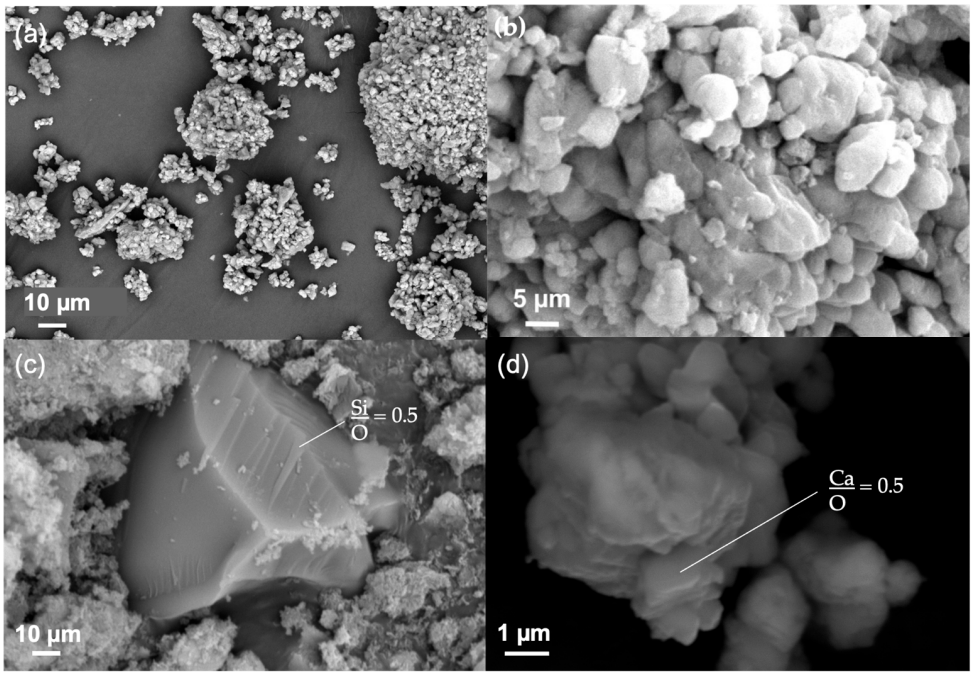

Figure 1. As-dried particles: (**a**,**b**) agglomerates, (**c**) SiO_2, (**d**) stack of $Ca(OH)_2$ platelets.

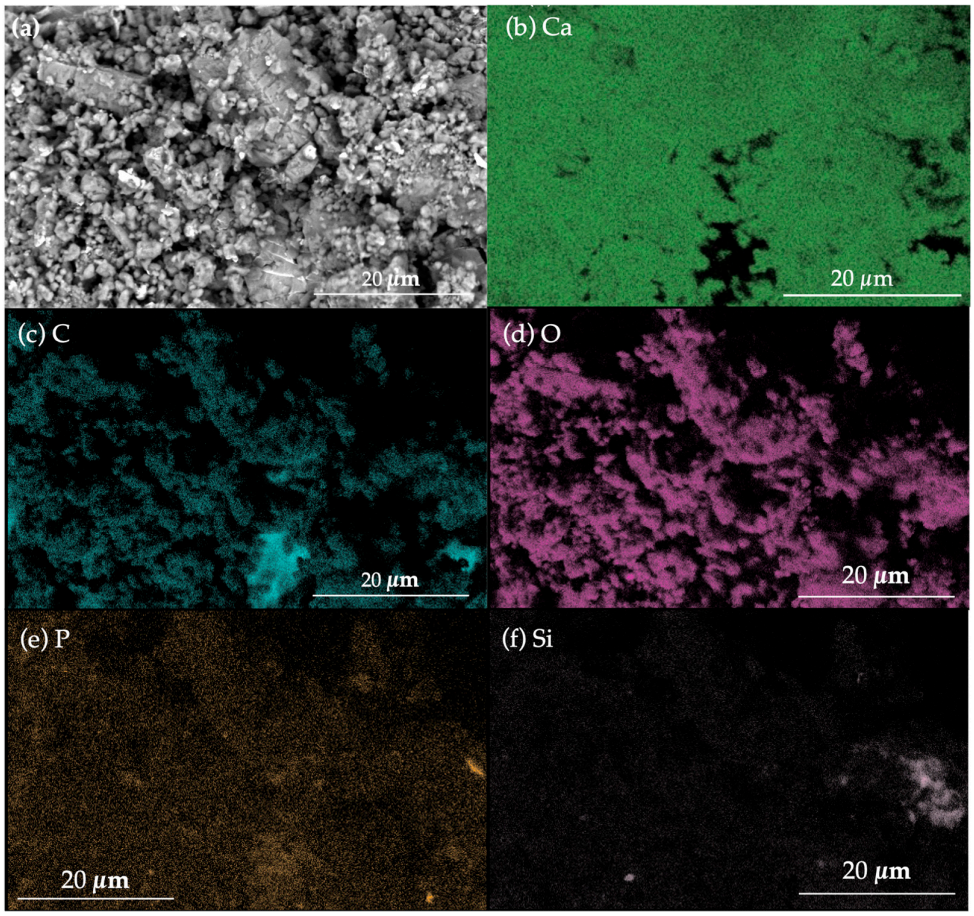

Figure 2. Elemental distribution in a dry powder sample: (**a**) mix secondary/backscattered electron image and distribution maps of (**b**) calcium, (**c**) carbon, (**d**) oxygen, (**e**) phosphorous, and (**f**) silicon.

The elemental maps clearly indicate that calcium and carbon dominate the composition, confirming the prevalence of calcite in the sludge and justifying its use as the primary precursor in subsequent mechanochemical reactions.

3.2.2. Chemical Composition and Crystalline Phases Present

The Raman spectrum of dry sludge particles (Figure 3a) is dominated by the strong sharp band around 1086 cm^{-1}, which corresponds to the fingerprint vibration mode of calcite. Weaker bands around 710 cm^{-1}, 525, and 447 cm^{-1} and lattice modes around 370, 280, and 154 cm^{-1}, often observed in $CaCO_3$ polymorphs, are also present [58]. Bands corresponding to SiO_2 (quartz polymorph) were identified around 1162, 1053, 810, 524, and 450 cm^{-1}. The characteristic vibration modes of $Ca(OH)_2$ are also present at 367 and 680 cm^{-1}. Finally, the Raman peak around 958 cm^{-1} is in good agreement with the main Raman band of crystalline hydroxyapatite [59]. The spectrum of the H_3PO_4 commercial aqueous solution (Figure 3b) is consistent with the characteristic vibration modes of solvated orthophosphoric acid, with bands around 355, 407, and 486 cm^{-1} (P-O bending) and 912 and 1083 cm^{-1} (P-O stretching) [60].

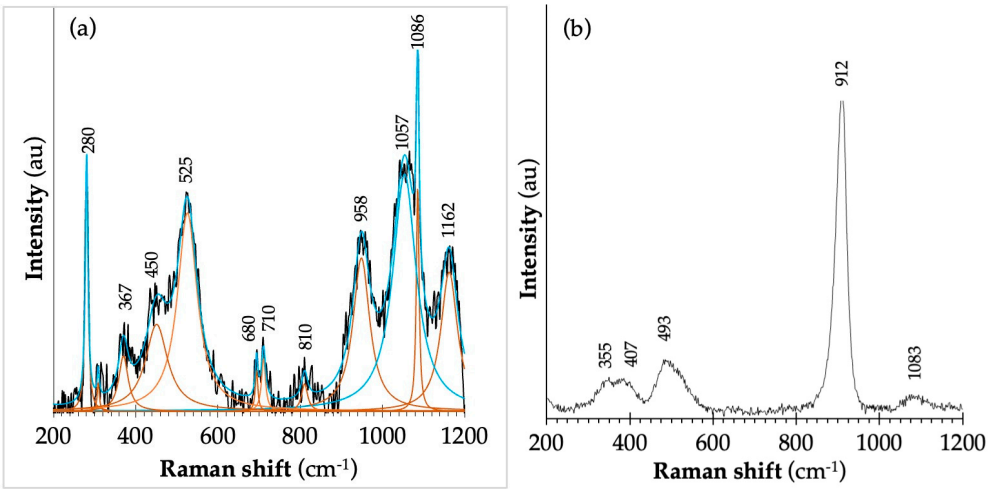

Figure 3. Raman spectra of (**a**) sludge particles — after background removal, — Lorentzian peak fit, and — peak deconvolution, and (**b**) commercial H_3PO_4 aqueous solution.

Raman data were importantly complemented by XRD results of the dry sludge (Figure 4), which confirm the detected calcium phosphate as hydroxyapatite (HA) and calcite as the only $CaCO_3$ polymorph present. Phase identification indicates that the phases are non-stoichiometric: HA is type-B carbonate-substituted (B-HA) [61], with refined structural formula $Ca_{10}(PO_4)_{5.83}(CO_3)_{0.17}(OH)_{2.00}$; calcium in $CaCO_3$ is partially substituted by Mg (Mg-calcite) [62], with refined composition $Ca_{0.936}Mg_{0.064}CO_3$. All diffraction peaks are sharp and well defined, and no amorphous hump is visible at low 2q values, demonstrating the high crystallinity of the material. The most intense and numerous peaks correspond to calcite reflexions. HA is identified by a small number of low intensity peaks, indicating its presence in a much smaller amount. Also, neither silica, portlandite (both detected by Raman spectroscopy), nor other crystalline phases were identified within the diffractometer detection limit. Rietveld quantification of the crystalline phases present rendered a sample composition of 98.8 ± 0.1 wt% Mg-calcite and 1.2 ± 0.1 wt% carbonated HA (these values were used from here onward).

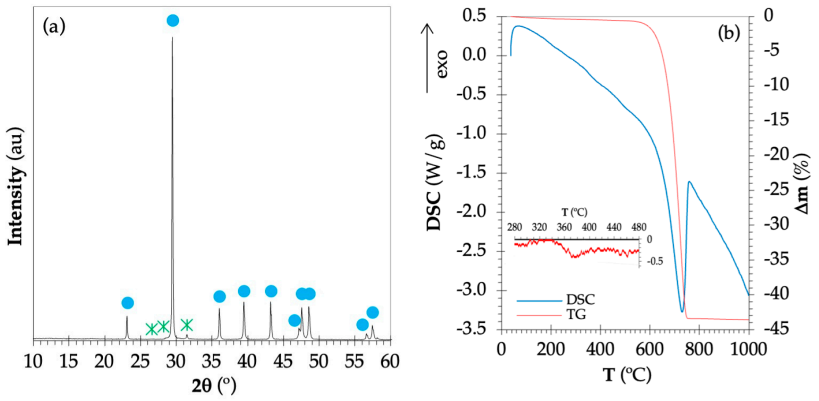

Figure 4. Characterization of dry sludge powder. (**a**) XRD results displaying • alcite (cod file 9001297) and ✳ HA (cod file 9003548). (**b**) Simultaneous DSC/TG curves of powder heated up to 1000 °C at 10 °C/min, including a magnification of the 280–480 °C temperature range.

The obtained DSC curve (Figure 4) displays one large and well-defined endothermal peak with onset at 570 °C (peak maximum around 730 °C), together with a shallow and broad endothermal signal with onset at approx. 280 °C (peak maximum around 398 °C). $Ca(OH)_2$ identified via Raman spectroscopy was not detected by XRD, and a clear thermal signal corresponding to its dehydration to CaO also could not be detected. No clear peak was identified in the expected 450–550 °C range [63], although there appears to be a very shallow endothermic event with a peak maximum around 550 °C. Yet, no distinct mass loss segment in that range could be quantified, likely due to the very low concentration of $Ca(OH)_2$ [64]. The endothermal effect with onset at approx. 280 °C is expected to correspond to the removal of physically bound water trapped in particle agglomerates or internal pores and not to a phase transition [64]. It spreads over a wide temperature range (approx. 280–480 °C) and corresponds to a mass loss around 0.5 wt%. At higher temperature, $CaCO_3$ decomposes (3), accompanied by the release of 43.5 wt% CO_2 (based on $CaCO_3$ dry weight).

$$CaCO_3 \rightleftarrows CaO + CO_2 \quad (3)$$

A straightforward calculation using mass loss values and reaction (3) indicates that the composition of the sludge powder is approx. 97.8 wt% $CaCO_3$ (corresponding to 39.2 wt% Ca) and 0.5 wt% physically bound water. The remaining 1.7 wt% are suggested to correspond to hydroxyapatite, which is thermally stable in the tested temperature range [59] and thus does not display any thermal effect.

Together, the XRD and DSC/TG results validate that calcite is the major phase, with minor hydroxyapatite present, providing the basis for controlled phase transformation during milling.

3.3. Characterization of Milled Powders

3.3.1. Particles' Morphology

Milling imposes significant changes in particle size, morphology, and phase composition compared to the starting as-dried material. Particle size consistently decreases, from a starting d_{50} value around 1132 nm, with increasing milling time (Figure 5a). Particle size step decreases to 285 nm in the first 5 min of milling (74.8% size reduction). Increasing milling time leads to continuous size reduction, but overall, a size decrease of only 16% is achieved on milling from 5 to 650 min (d_{50} ~ 240 nm) duration. All batches display a standard deviation value higher than their median particle size, indicating a broad and skewed size distribution [65]. For this reason, the chosen indicator to measure the distribution broadness was instead size span (Figure 5b) [65]. Particle size span step increases from

the initial value of 2.4 in as-dried powder up to 3.5 after 5 min of milling; afterwards, it continuously decreases to a minimum of 1.4 (650 min milling duration).

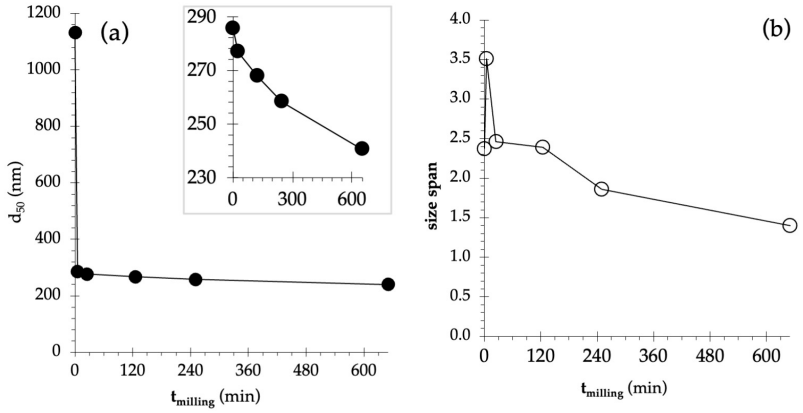

Figure 5. Effect of milling time on particle size distribution: evolution of (**a**) d_{50} and (**b**) size span.

These results are in good agreement with SEM observation (Figure 6). Milling as-dried particles (Figure 6a) during 5 min (Figure 6b) has a pronounced effect upon particle size: overall particle size apparently decreases as a result of the milling action. Yet, tabular micrometric particles, much bigger than average, are abundant. DCPD powder morphology is strongly affected by solution pH, and such plate-like particles require high pH conditions [66]. Further increasing milling time to 25 min (Figure 6d), 125 min (Figure 6d), 250 min (Figure 6e), and 650 min (Figure 6f) continuously decreases size distribution broadness. In particular, size span decreases 32% when milling time increases from 5 min (3.51) to 125 min (2.39) and decreases another 25% when the milling duration is between 125 min and 650 min (1.40).

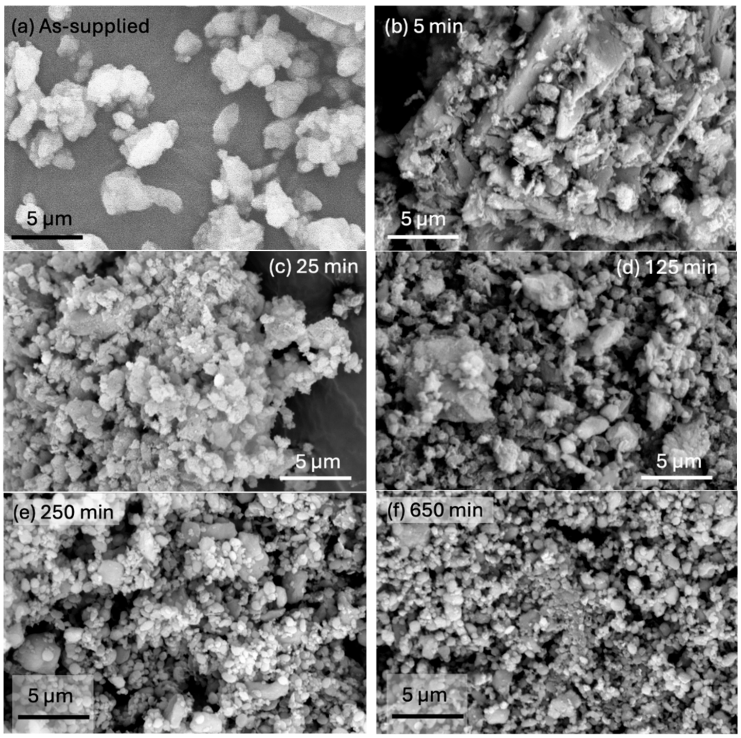

Figure 6. Sludge powder milled during (**a**) as supplied, (**b**) 5, (**c**) 25, (**d**) 125, (**e**) 250 and (**f**) 650min.

The SEM observations demonstrate a progressive reduction in particle size and narrowing of the size distribution with increasing milling time, indicating effective mechanical activation of the material.

3.3.2. Phase Transformation During Milling

Raman spectroscopy (Figure 7a) and XRD (Figure 7b) results show significant changes in milled powders' phase composition with increasing milling time. The DCPD Raman fingerprint (two bands, around 986 and 878 cm^{-1} [59]), not present in the as-dried sludge spectrum, emerges after milling during 5 min, which can be confirmed in the diffractogram. Apparently, this is the milling duration rendering the maximum amount of DCPD (although higher concentration could have been present during a shorter time). At 25 min (at most), DCPD concentration significantly decreases it is apparently residual at 125 min and fully consumed between 125 and 250 min (Table 2).

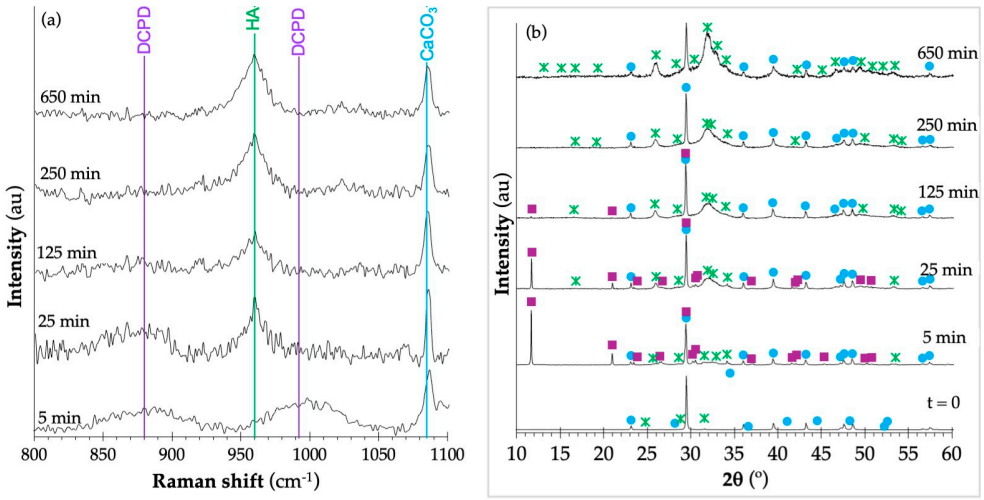

Figure 7. Phase transformation as a function of milling time. (**a**) Phases' chemical composition. (**b**) Crystalline phases present. • calcite (cod 9001297), ✳ HA (cod 9003548), and ■ DCPD (cod 1533075).

Table 2. Rietveld quantification and reliability factors of crystalline phases identified in milled powders.

$t_{milling}$ (min)	Phase (wt%)			Reliability Factors			
	Calcite	HA	DCPD	R_{wp}	R_{exp}	χ^2	GoF
0	98.8 ± 0.1	1.2 ± 0.1	-	8.06	5.74	1.9717	1.4012
5	40.1 ± 0.6	38.8 ± 0.7	21.1 ± 0.7	12.1	6.35	4.0063	2.0016
25	26.1 ± 0.4	67.6 ± 0.4	6.3 ± 0.2	9.08	6.61	1.8870	1.3717
125	21.6 ± 0.3	77.6 ± 0.4	0.8 ± 0.1	7.75	6.58	1.3872	1.1778
250	19.1 ± 0.4	80.9 ± 0.4	-	7.60	6.40	1.4102	1.1875
650	13.6 ± 0.4	86.4 ± 0.4	-	7.89	6.05	1.7008	1.3041

R_{wp}: weighted profile; R_{exp}: expected profile; χ^2: agreement between experimental and calculated diffraction. Data; GoF: goodness of fit.

In the studied milling time range, calcite and HA are always present (Table 2). Calcite continuously decreases from a maximum of 98.8 wt% in the as-dried sludge to a minimum of 13.6 wt% after 650 min (Figure 8a). HA follows the inverse trend, increasing from 1.2 wt% to 86.4 wt% (Figure 8b), respectively. The best fit for both processes is a logarithmic function, displayed in Figure 8a,b. The concentration of DCPD, which is stable during milling from at least 5 min (21.1 wt%) to 125 min (0.8 wt%), continuously decreases, also following a

logarithmic trend (Figure 8a). DCPD, HA, and calcite coexist up to at least 125 min (Table 2). For the remaining tested milling times, both calcite and HA are present, and only biphasic domains are achieved.

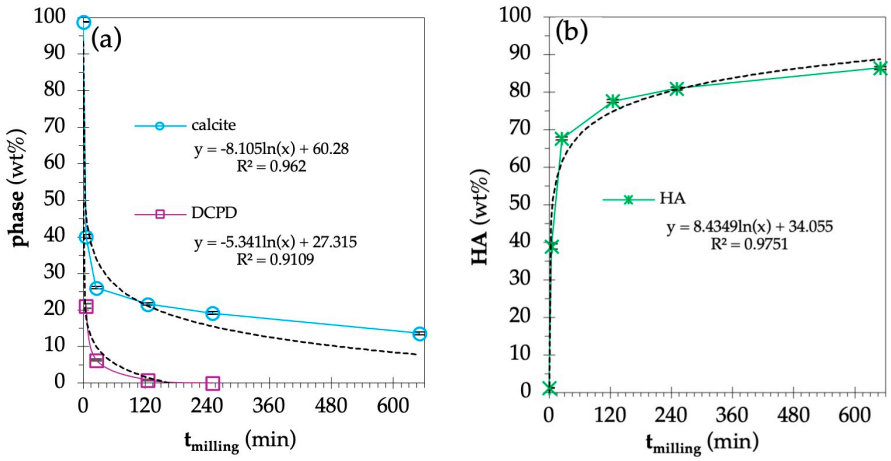

Figure 8. Evolution of phase concentration with milling time: (**a**) calcite and DCPD; and (**b**) HA. The equation that best fits the progress of each phase with increasing milling time is shown.

The evolution of calcite, DCPD, and hydroxyapatite contents follows a logarithmic trend, confirming that the mechanochemical process drives a time-dependent transformation towards a predominant hydroxyapatite phase.

4. Discussion

Previous studies by the authors [36,37] have demonstrated that mechanochemical processing provides sufficient energy to promote the room-temperature formation of the thermodynamically stable calcium phases within the $CaCO_3$-H_3PO_4-H_2O system. Building upon this foundation, the present work confirms that industrial limestone sludge can serve as a sustainable calcium precursor for the mechanosynthesis of hydroxyapatite (HA), offering both environmental and economic advantages.

4.1. Limestone Sludge as Calcium Source for Bioceramics

The sludge used as calcium source was produced by processing Moleanos limestone (cutting, sawing, grinding, and polishing cycles and finishing operations) quarried at Batalha, Portugal. Sludge composition is a parameter of utmost importance for the quality of the recycled material [49]. The sludge was first scrutinized for heavy metals and other hazardous contaminants, whose presence is not uncommon in quarry sludge originating from natural (rocks) or anthropological sources (e.g., mining, pesticides) [66]. Their presence in the tested limestone was thus a major concern, considering that the produced calcium phosphates were envisioned to be used as bioceramics. Aluminum, sulfur, mercury, cadmium, and iron were detected (Table 1). Although their concentration appears to vary greatly in time, the Cd and Hg content are below the limit specified by ASTM for calcium phosphate bone substitutes (0.005 mg/g for both metals) [67] and would not thus be a barrier for the use of the studied limestone sludge in bone healing applications. A similar conclusion was also reached by other authors [46,49]. Also, no thermal events corresponding to the calcination of lubricants or other contaminants were detected by DSC/TG (Figure 4b). The ICP–OES analysis (Table 1) shows that the sulfur content in the limestone sludge varies between 1.09 and 3.58 mg/g. Although this variation reflects the heterogeneity of the sludge source, the detected levels remain within the range typically reported for natural limestone residues and are not expected to interfere significantly with

the mechanochemical synthesis of hydroxyapatite. It is quite possible that S identification is connected with the presence of SO_4^{2-} in the calcareous deposit. SO_4^{2-} is one of the trace ions that improves the bone function of calcium phosphates [7]. Furthermore, no sulfate or sulfide phases were identified by XRD or Raman spectroscopy, and no microstructural defects or cracks were observed (by SEM) in the milled powders. This indicates that the sulfur present is either structurally bound in trace amounts within the carbonate matrix, or removed during milling as volatile species, without compromising the chemical or mechanical performance of the final product. Nonetheless, future work will further investigate the possible effects of residual S on the sintering behavior and long-term stability of the bioceramic.

The calcite phase in the sludge is highly crystalline (Figure 4a) and contains magnesium. A concentration of 98.8 wt% calcite was calculated by Rietveld refinement, corresponding to the structural formula $Ca_{0.936}Mg_{0.064}CO_3$. The corresponding calcium outcome of this $CaCO_3$ amount is 39.2 wt%—available to the mechanochemical reaction. It should be mentioned that this value is higher than that provided by other sustainable calcium sources such as chicken eggshell (38.5 wt% Ca^{2+}) or cuttlefish (37.7 wt%) [36]. Carbonated hydroxyapatite and trace quartz and portlandite were also detected in the slurry. These minor phases are not unusual in calcareous deposits [68]. Quartz originates from the quarry rock or from clay weathering and is a common contamination in calcite deposits [58]. $Ca(OH)_2$ is suggested to result from exposure to the atmosphere or reaction with liquid water: CaO present on the surface at some point strongly reacts with water, leading to the formation of covalent OH bonds [3,68]. Because Raman spectroscopy is very sensitive to molecular vibrations, even small amounts of CH or SiO_2 not detected within the diffractometer LOD are enough to significantly contribute to Raman spectra [69]. It should be mentioned that portlandite was also not confirmed by DSC/TG, with no thermal signal in the expected 450–550 °C temperature range [63]. The presence of hydroxyapatite is common in calcareous geological deposits, indicating the presence of a fossil-bearing/marine sediment layer or diagenetic phosphate enrichment [58,68]. The identified HA is non-stoichiometric and substituted (refined structural formula $Ca_5H_{1.44}O_{13.012}P_{2.928}$). This suggests a diagenesis process with $CaCO_3$, which partially replaces or associates with the PO_4^{3-} group in hydroxyapatite, rendering type-B HA [58,68]. While HA concentration in the sludge is ~1.2 wt% as determined by Rietveld refinement, 1.7 wt% resulted from TG. The discrepancy is expected to result from the presence of 0.45 wt% interstitial water in particle agglomerates (not accounted for in XRD refinement). The presence of trace ion substitutions is of major importance for the use of produced HA as a bioceramic. In fact, while commercially available synthetic HAs are stoichiometric, biological HA is poorly crystalline, calcium-deficient, and incorporates trace amounts of a variety of substitute ions (e.g., Mg^{2+}, Sr^{2+}, F^-, CO_3^{2-}) at Ca^{2+}, PO_4^{3-}, and/or OH^- sites [70]. Their presence does not alter the basic crystallographic characteristics of HA but directly influences biochemical reactions linked to the development, metabolism, and overall lifecycle of hard tissues [44]. As a result, the success of synthetic HA is relative concerning physiological tolerance, biocompatibility, and long-term stability. Development of non-stoichiometric, substituted versions is of great interest to the biomedical community [25]. Importantly, when the precursor reagents used to produce synthetic HA contain trace ions, these will remain in the structure of the reaction product [7]. This maximizes similarity with human hard tissues, thereby improving biological performance of the implant material [70].

As reported in Table 1, the concentration of potentially hazardous elements in the Moleanos limestone sludge is extremely low: Cd < 0.00042 mg/g, Hg < 0.00059 mg/g, and Fe and Al below 0.25 mg/g. These values are below the regulatory limits defined for inert materials according to European Directive 2003/33/EC and well under the threshold

established by ASTM for bone substitute materials. Therefore, the risk of metal leaching into the environment is negligible. Moreover, the mechanochemical processing route proposed in this work operates as a closed, solvent-free system where reagents are fully incorporated into the solid phase. The final bioceramic product (hydroxyapatite) is a chemically stable, low-solubility material that effectively immobilizes any trace metallic ions within the crystal lattice, further minimizing leaching potential. In addition, no effluents or liquid waste are produced during the process—only solid powders, which are recovered and reused. Thus, the proposed method is environmentally safe and contributes to sustainable waste management by converting a potentially polluting residue into a stable, value-added product.

Thus, the combined use of mechanosynthesis and limestone sludge in this work appears to be a viable route for direct production of synthetic HA with a crystalline structure and composition similar to human hard tissues.

4.2. Mechanochemical Reaction Pathway and Phase Evolution

While solids in the as-supplied sludge comprise 98.8 wt% calcite and 1.2 wt% HA, milling has a significant effect upon the phases present and their concentration. The amount of calcite continuously decreases with increasing milling time (Figure 8a), but full depletion is not reached in the tested time range. Calcite continuous consumption is accompanied by DCPD formation (with onset in the $0 < t_{milling} \leq 5$ min range), continuous decrease, and full consumption ($125 < t_{milling} < 250$ min) (Figure 8a). Simultaneously, HA concentration continuously increases with increasing milling time (Figure 8a), although a monophasic HA domain was not achieved within the tested milling time.

CaP mechanosynthesis in the $CaCO_3$-H_3PO_4-H_2O system occurs through the same sequence of dissolution–reprecipitation reactions than conventional wet synthesis [71], thoroughly described in the literature, e.g., [40,42,72–74]. In conventional synthesis, direct HA precipitation from solution is extremely slow [40,72], and calcium consumption only reaches completion if significant energy input is provided [59]. In high-energy milling, this is surpassed by the significant reactivity increase at room temperature [38,39]. When $CaCO_3$ and H_3PO_4 are mixed in solution, the synthesis reaction is triggered: dissociation of the triprotic phosphoric acid takes place, with the relative concentration of the protonated acid form and of the conjugated phosphate base depending on solution pH (3); acid attack results in $CaCO_3$ dissolution in water (3), and calcium and phosphate ions enter the solution in a proportion that depends on pH [73]. Depending on their pH, the calcium- and phosphate-containing solutions can be supersaturated with respect to different CaP phases [72]. After phase precipitation, equilibrium is expected to be reached through a sequence of reactions that culminates in the formation of the thermodynamically stable phase for the system [42,72]. In the current study, the Ca/P =1.67 molar ratio composition is expected to promote hydroxyapatite formation [42,72].

$$\begin{array}{c} p_{ka1} = 2.12 \qquad p_{ka2} = 7.21 \qquad p_{ka1} = 12.67 \\ H_3PO_4 \rightleftharpoons H_3PO_4^- + H^+ \rightleftharpoons HPO_4^{2-} + 2H^+ \rightleftharpoons PO_4^{3-} + 3H^+ \end{array} \quad (4)$$

$$2H^+ + CaCO_3 \rightarrow Ca^{2+} + H_2O + CO_2 \quad (5)$$

Attained results (Figure 7) show that the DCPD stability domain corresponds to a milling duration between approx. 5 and 25 min, with decreasing concentration with increasing milling time (Figure 8a). In that time range, HA is always present, and its concentration increases with increasing milling time (Figure 8b). Furthermore, that increase is much more significant up to around 25 min (Figure 8b). This suggests that DCPD (Ca/P =1.0) was the first calcium phosphate to precipitate from solution (6) [72,74], a

$tt_{milling} \leq 5$ min. DCPD functions as an intermediate phase in HA production (7) [72] at least as long as pH < 8. Above pH 8, reaction (8) HA is able to precipitate directly from the solution [72].

$$\underset{}{4.2 \leq pH \leq 6.5}$$
$$Ca^{2+} + H_2PO_4^- + OH^- + H_2O \rightleftharpoons \underset{(DCPD)}{CaHPO_4 \cdot 2H_2O} \quad (6)$$

$$\underset{}{pH \leq 4.2}$$
$$\underset{(DCPD)}{CaHPO_4 \cdot 2H_2O} + 4OH^- \rightleftharpoons \underset{(HA)}{Ca_{10}(PO_4)_6(OH)_2} + 4H_2PO_4^- + +22H_2O \quad (7)$$

$$\underset{}{8.0 < pH < 10.0}$$
$$Ca^{2+} + 6PO_4^{3-} + 2OH^- \rightleftharpoons \underset{(HA)}{Ca_{10}(PO_4)_6(OH)_2} \quad (8)$$

The pH value required to trigger each of these reactions is much higher than the value measured immediately after reagents' mixture (pH = 0.8). This suggests that continuous dissolution of calcite (3.2) is taking place at a sufficiently high rate to foster pH increase (i.e., higher than the rate of H^+ release in 3.1) [72]. However, reaction (4) appears to stop between 25 and 125 min, and from then onwards, reaction (5) can only progress while DCPD is available as reagent. The very slow HA concentration increase (and calcite decrease) at higher milling duration indicates that at milling times higher than 125 min, reaction (2) is incomplete, and reaction (6) takes place to a small extent. This is suggested to result from insufficient water initially present in the system (50 wt% based on dry solids) [35], although it surpasses the stoichiometric requirement for the completion of reaction (4). The influence of water on HA formation is very well known [75]. (For example, solid-state synthesis of HA only takes place in the presence of at least 500 mmHg water partial pressure [75].) To the best of the authors' knowledge, there is no reference value for water concentration in wet synthesis, although the relative amount of solid and liquid phases originally present is bound to affect the dissolution–reprecipitation chemistry in the system [41]. The outcome of mechanosynthesis is additionally influenced by the amount of water because it provides the environment for dissolution of particles' surface, species transport, and precipitation/recrystallization reactions, establishing the flow and transport interaction regime between the solid phases involved in the mechanochemical reactions [38]. In the current work, A single $CaCO_3$-H_3PO_4-H_2O formulation was tested, complying with the Ca/P = 1.67 molar ratio of hydroxyapatite and containing a total 50 wt% H_2O. Expectedly, a higher water amount would foster progress of reactions (4) and (5) and extend the DCPD stability domain (4), making it available to intermediate HA formation at longer times, eventually resulting in the completion of reaction (6) [35]. Figure 9a shows a schematic representation of the proposed mechanochemical reaction path in the sludge-based system.

Finally, the inherent reduced size of precipitate particle size allows the production of CaP particles with submicron/nanometric size, which have been reported to exhibit enhanced resorbability, bioactivity, and release of calcium ions when compared to micrometric CaP commercially available from conventional synthesis [65].

The progressive transformation from calcite to hydroxyapatite was clearly evidenced by XRD and Raman spectroscopy. Dicalcium phosphate dihydrate (DCPD) appeared as a transient phase at early milling stages (≤25 min), confirming that mechanochemical reactions proceed through a dissolution–reprecipitation mechanism similar to wet synthesis routes. As milling time increased, DCPD was gradually consumed while HA concentration followed a logarithmic growth, indicating that reaction kinetics are controlled by surface activation and diffusion limitations. This sequential conversion—calcite → DCPD

→ HA—demonstrates that mechanosynthesis effectively overcomes the kinetic barriers associated with low-temperature reactions in the $CaCO_3$–H_3PO_4–H_2O system. The formation of a non-stoichiometric, carbonate-substituted HA is particularly relevant, as it mimics the composition of biological apatite in human bone and teeth, improving bioresorbability and cell affinity compared to stoichiometric synthetic HA.

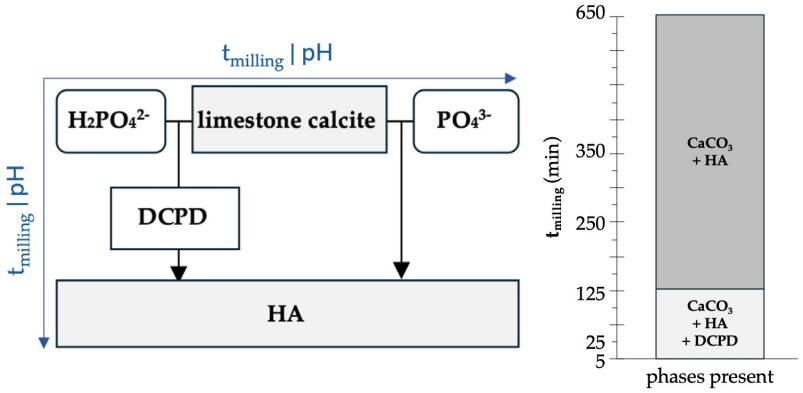

Figure 9. Mechanochemical reaction between limestone sludge and H_3PO_4 solution: (**a**) reaction path; (**b**) phases' stability domain over time.

4.3. Microstructural and Functional Implications

SEM analysis revealed that extended milling (≥250 min) reduced particle size to the submicron scale ($d_{50} \approx 240$ nm), producing homogeneous and fine powders with narrow size distribution. Such nanoscale morphology enhances bioactivity and resorption kinetics in biomedical applications, while providing a larger reactive surface area for ion exchange and catalysis in non-biomedical uses. The incorporation of trace ions such as Mg^{2+}, Sr^{2+}, and CO_3^{2-}—naturally present in the sludge—introduces lattice substitutions that are known to increase osteoconductivity and biocompatibility. This inherent compositional advantage distinguishes the recycled product from HA obtained from pure laboratory reagents.

4.4. Economic and Environmental Feasibility

Although a complete techno-economic assessment is beyond the scope of this paper, preliminary considerations indicate strong economic feasibility. Limestone sludge is a low-cost, highly available by-product whose management currently represents a significant expense for stone processing companies. Reusing it as a raw material not only eliminates disposal costs but also substitutes expensive analytical-grade calcium sources. Mechanosynthesis further enhances the process economy by operating at room temperature and atmospheric pressure, eliminating the need for calcination or solvent-based reactions. The entire process—high-energy milling followed by drying—is simple, scalable, and compatible with existing industrial milling infrastructure. The energy savings, coupled with waste reduction, make this approach both economically and environmentally advantageous. The environmental safety of the proposed recycling route was also evaluated through chemical characterization of the sludge. The concentrations of potentially hazardous elements such as Cd, Hg, and Fe were found to be well below the limits defined for inert materials and biomedical-grade calcium phosphates. Moreover, mechanochemical synthesis occurs under closed, solvent-free conditions, producing a solid hydroxyapatite phase that immobilizes trace metals within a stable crystalline lattice. Consequently, the risk of leaching or secondary contamination is minimal. This confirms that the transformation

of limestone sludge into bioceramics not only provides a sustainable resource but also eliminates the environmental burden associated with landfill disposal.

4.5. Broader Context and Future Work

It should be emphasized that hydroxyapatite (HA) bioceramics were successfully synthesized from the Moleanos limestone sludge via mechanochemical processing. The formation of HA was confirmed by both XRD and Raman spectroscopy, which showed the progressive transformation of calcite into hydroxyapatite through a transient DCPD phase, reaching 86.4 wt% HA after 650 min of milling. The obtained powders exhibit the characteristic morphology and crystallinity of calcium phosphate bioceramics. Although the present work focuses on the synthesis and characterization of the bioceramic powder, further developments are underway to consolidate these powders into sintered bodies and evaluate their mechanical and biological performance.

The findings of this study align with the principles of circular economy and sustainable materials engineering. By valorizing limestone sludge into high–added-value bioceramics, this work contributes to reducing the environmental footprint of the natural stone industry while promoting resource efficiency. Future research will focus on the following:

- Quantitative assessment of process scalability and energy demand.
- Sintering behavior and mechanical performance of HA ceramics derived from sludge.
- In vitro biocompatibility tests to confirm biomedical suitability.
- Detailed techno-economic and lifecycle analyses to validate the industrial potential of the proposed process.

5. Conclusions

Limestone sludge coming from limestone processing operations is produced in vast amounts worldwide and poses a massive environmental challenge. However, this also makes it highly available as a secondary source. This work envisions limestone sludge as a sustainable raw material that can feasibly be recycled into bioceramics with high added value.

The proposed mechanochemical recycling route offers several economic advantages compared to conventional synthesis of hydroxyapatite from analytical-grade reagents. Limestone sludge is an abundant industrial by-product that currently has negligible market value and high disposal costs. Its reuse as a calcium source therefore represents direct savings in the cost of raw materials and waste management. Moreover, mechanosynthesis occurs at room temperature and atmospheric pressure, requiring no calcination or sintering stages, which significantly reduces energy consumption and operational costs relative to traditional wet or solid-state synthesis methods. Additionally, the simplicity of the process—based on direct high-energy milling and drying—makes it easily scalable and compatible with existing industrial milling equipment, further supporting its potential for large-scale implementation. In contrast to most previous studies that incorporated limestone or marble waste into low-value construction materials (e.g., cement, mortar, or ceramic bricks), the present work introduces a novel upcycling strategy that converts limestone sludge into a high-value bioceramic. By employing mechanochemical synthesis at room temperature, the process eliminates the need for high-temperature calcination or solvent-based reactions, significantly reducing energy input and environmental footprint. This approach expands the traditional concept of waste reuse in the construction industry, demonstrating that stone processing residues can serve as raw materials for advanced materials engineering, particularly in the biomedical field.

Obtained results demonstrate limestone sludge's potential as a calcium precursor in the synthesis of hydroxyapatite and the ability of high-energy milling as the corresponding

processing route. This opens a window of opportunity for the development of a fast and cost-effective HA production method—very promising from the sustainability perspective. In summary, while a full techno-economic assessment will be the focus of future work, preliminary considerations clearly indicate that the proposed process is economically viable, offering both cost reduction and environmental benefits consistent with circular economy principles.

Author Contributions: Conceptualization, M.G. and S.B.; methodology, J.C., M.G., S.B. and T.S.; validation, C.A., M.G., M.M.G., R.B., R.G. and S.B.; investigation, J.C., M.G., S.B. and T.S.; writing—original draft preparation, J.C. and M.G.; writing—review and editing, C.A., J.C., M.G., M.M.G., R.B., R.G. and S.B.; project administration, S.B.; funding acquisition, M.G. and S.B. All authors have read and agreed to the published version of the manuscript.

Funding: This work was funded by national funds through FCT—Fundação para a Ciência e a Tecnologia, I.P., within the scope of the project UID/04292/MARE—Centro de Ciências do Mar e do Ambiente; LSRE-LCM, UIDB/50020/2020 (DOI: 10.54499/UIDB/50020/2020) and UIDP/50020/2020 (DOI: 10.54499/UIDP/50020/2020); ALiCE, LA/P/0045/2020 (DOI: 10.54499/LA/P/0045/2020); LA/P/0069/2020 (ARNET); and UIDB/04540/2020 (CeFEMA) under project PTDC/ECI-COM-28308/2017. It was also funded by the Mobilizing Agenda Sustainable Stone by Portugal—Valorization of Natural Stone for a digital, sustainable and qualified future, project number 02-C05-i01.02-2022.PC644943391-00000051, cofinanced by PRR (Recovery and Resilience Plan) funded by the European Union (NextGenerationEU). Tomás Seixas is grateful to FCT for the Doctoral Grant 2022.10551.BD.

Data Availability Statement: The data are available upon request from the corresponding author.

Acknowledgments: The authors would like to thank MARFILPE for providing the Moleanos sludge used in this study. The authors are grateful to A.C. Ferro for assistance in XRD.

Conflicts of Interest: The authors declare no conflicts of interest.

References

1. Oates, J.A.H. *Lime and Limestone: Chemistry and Technology, Production and Uses*, 2nd ed.; John Wiley & Sons: Hoboken, NJ, USA, 2008.
2. Tazzini, A.; Gambino, F.; Casale, M.; Dino, G.A. Managing Marble Quarry Waste: Opportunities and Challenges for Circular Economy Implementation. *Sustainability* **2024**, *16*, 3056. [CrossRef]
3. Murali, G.; Wong, L.S.; Ramkumar, V.R.; Abid, S.R.; Karthik, S. From waste to resource recycled lime sludge: Sustainable low clinker cementitious binder, a comprehensive study on hydration, strength of concrete. *J. Build. Eng.* **2024**, *86*, 108935. [CrossRef]
4. Tennis, P.D.; Thomas, M.D.A.; Weiss, W.J.; Farny, J.A.; Giannini, E.R. *State-of-the-Art Report on Use of Limestone in Cements at Levels of Up to 15%*; PCA R&D Report SN3148.03; America's Cement Manufactures: Washington, DC, USA, 2024.
5. Scioti, A.; Bernardo, G.; Mecca, I.; Fatiguso, F. Characterization of Stone Waste Sludge and Preliminary Investigation on Green Materials Based on Traditional Lime Putty for Sustainable Construction. *Sustainability* **2024**, *16*, 9173. [CrossRef]
6. Mehta, D.; Palwal, D.; Sankhla, V.S. Marble Waste Management for Protection of Ecology and Environment. *Int. J. Innov. Sci. Eng. Technol.* **2020**, *7*, 2348–7968.
7. Baker, R.J.; Leeuwen, J.; White, D.J. *Applications for Reuse of Lime Sludge from Water Softening*; Final Report for TR-535; Iowa State University: Ames, IA, USA, 2005.
8. Liu, D.; Wang, Q.; Hu, A.; Wang, Z.; Zhang, Q.; Wang, L. Optimized model of sludge drying characteristics based on an experimental study of thickness, temperature, and humidity. *J. Clean. Prod.* **2023**, *429*, 139540. [CrossRef]
9. Dubey, R.K.; Bhatta, B.D. Chemical and Instrumental Analysis of Limestone and Red Clay from Makwanpur District for Cement Production. *J. Nepal Chem. Soc.* **2023**, *43*, 46–52. [CrossRef]
10. Onodagu, P.D.; Obi, K.O.; Aginam, C.H.; Okoye, M.U.; Chidolue, C.U. Understanding the Influence of Different Limestone Sources on Portland Limestone Cement Characteristics and Advancements in Green Cement. *Int. J. Recent Res. Civ. Mech. Eng.* **2024**, *11*, 39–47. [CrossRef]
11. Kakali, G.; Tsivilis, S.; Kolovos, K. Factors Affecting the Reactivity of the CaO-SiO_2-Al_2O_3-Fe_2O_3 Mixture. *Key Eng. Mater.* **2001**, *206–213*, 1899–1902. [CrossRef]

12. Chang, Z.; Long, G.; Xie, Y.; Zhou, J.L. Recycling sewage sludge ash and limestone for sustainable cementitious material production. *J. Build. Eng.* **2022**, *49*, 104035. [CrossRef]
13. Ganapathi, H.; Phukan, M. Environmental Hazards of Limestone Mining and Adaptive Practices for Environment Management Plan. In *Environmental Processes and Management*; Singh, R.M., Shukla, P., Singh, P., Eds.; Springer: Berlin/Heidelberg, Germany, 2020; pp. 121–134. [CrossRef]
14. Klemm, A.; Wiggins, D. Sustainability of natural stone as a construction material. In *Sustainability of Construction Materials*; Khatib, J.M., Ed.; Woodhead Publishing: Cambridge, UK, 2016; pp. 283–308. [CrossRef]
15. Ziemkiewicz, P.F.; Brant, D.L.; Skousen, J.G. ACID MINE DRAINAGE TREATMENT WITH OPEN LIMESTONE CHANNELS. *J. Am. Soc. Min. Reclam.* **1996**, *1996*, 367–374. [CrossRef]
16. Ziemkiewicz, P.F.; Skousen, J.G.; Simmons, J. Long-term performance of passive acid mine drainage treatment systems. *Mine Water Environ.* **2003**, *22*, 118–129. [CrossRef]
17. Al-Hamaiedeh, H.D. Reuse of Marble Sludge Slime in Ceramic Industry. *Jordan J. Civ. Eng.* **2010**, *4*, 264–274.
18. Amin, S.K.; Abdel Hamid, E.M.; El-Sherbiny, S.A.; Sibak, H.A.; Abadir, M.F. The use of sewage sludge in the production of ceramic floor tiles. *HBRC J.* **2018**, *14*, 309–315. [CrossRef]
19. Careddu, N.; Siotto, G.; Siotto, R.; Tilocca, C. From landfill to water, land and life: The creation of the Centre for stone materials aimed at secondary processing. *Resour. Policy* **2013**, *38*, 258–265. [CrossRef]
20. Khan, Z.; Gul, A.; Shah, S.A.A.; Qazi, S.; Wahab, N.; Badshah, E.; Naqash, T.; Shahzada, K. Utilization of Marble Wastes in Clay Bricks: A Step towards Lightweight Energy Efficient Construction Materials. *Civ. Eng. J.* **2021**, *7*, 1488–1500. [CrossRef]
21. Walker, I.; Bell, R.; Rippy, K. Mineralization of alkaline waste for CCUS. *npj Mater. Sustain.* **2024**, *2*, 28. [CrossRef]
22. Chai, S.Y.W.; How, B.S.; Chin, M.Y.; Ngu, L.H. Utilization of accelerated weathering of limestone captured carbon dioxide (CO_2) with cement kiln dust to produce building material. *J. Clean. Prod.* **2024**, *468*, 143047. [CrossRef]
23. Yurdakul, M. Natural stone waste generation from the perspective of natural stone processing plants: An industrial-scale case study in the province of Bilecik, Turkey. *J. Clean. Prod.* **2020**, *276*, 123339. [CrossRef]
24. Dorozhkin, S. Medical Application of Calcium Orthophosphate Bioceramics. *BIO* **2011**, *1*, 1–51. [CrossRef]
25. Dorozhkin, S.V. Bioceramics of calcium orthophosphates. *Biomaterials* **2010**, *31*, 1465–1485. [CrossRef] [PubMed]
26. Dorozhkin, S.V. Calcium Orthophosphate ($CaPO_4$) Scaffolds for Bone Tissue Engineering Applications. *J. Biotechnol. Biomed. Sci.* **2018**, *1*, 25–93. [CrossRef]
27. LeGeros, R.Z. Properties of Osteoconductive Biomaterials: Calcium Phosphates. *Clin. Orthop. Relat. Res.* **2002**, *395*, 81–98. [CrossRef]
28. Diez-Escudero, A.; Espanol, M.; Ginebra, M.P. High-aspect-ratio nanostructured hydroxyapatite: Towards new functionalities for a classical material. *Chem. Sci.* **2024**, *15*, 55–76. [CrossRef] [PubMed]
29. Mondal, S.; Park, S.; Choi, J.; Vu, T.T.H.; Doan, V.H.M.; Vo, T.T.; Lee, B.; Oh, J. Hydroxyapatite: A journey from biomaterials to advanced functional materials. *Adv. Colloid Interface Sci.* **2023**, *321*, 103013. [CrossRef] [PubMed]
30. Nayak, A.; Bhushan, B. Hydroxyapatite as an advanced adsorbent for removal of heavy metal ions from water: Focus on its applications and limitations. *Mater. Today Proc.* **2021**, *46*, 11029–11034. [CrossRef]
31. Jemli, Y.E.L.; Abdelouahdi, K.; Minh, D.P.; Barakat, A.; Solhy, A. Synthesis and Characterization of Hydroxyapatite and Hydroxyapatite-Based Catalysts. In *Design and Applications of Hydroxyapatite-Based Catalysts*; Wiley: Hoboken, NJ, USA, 2022; pp. 19–72. [CrossRef]
32. Munirathinam, R.; Minh, D.P.; Nzihou, A. Calcium phosphates as a novel support material for catalysis in Fischer-Tropsh synthesis. *J. Fundam. Renew. Energy Appl.* **2017**, *7*, 51. [CrossRef]
33. Jaffar, F.H.; Othman, M.H.D.; Ismail, N.J.; Puteh, M.H.; Kurniawan, T.A.; Abu Bakar, S.; Abdullah, H. Hydroxyapatite-based materials for adsorption, and adsorptive membrane process for heavy metal removal from wastewater: Recent progress, bottleneck and opportunities. *J. Taiwan Inst. Chem. Eng.* **2024**, *164*, 105668. [CrossRef]
34. Turck, D.; Castenmiller, J.; De Henauw, S.; Hirsch-Ernst, K.I.; Kearney, J.; Maciuk, A.; Mangelsdorf, I.; McArdle, H.J.; Naska, A.; Pelaez, C.; et al. Safety of 2′-fucosyllactose/difucosyllactose mixture as a novel food pursuant to Regulation (EU) 2015/2283. *EFSA J.* **2019**, *17*, e05717. [CrossRef]
35. Ferro, A.C.; Guedes, M. Mechanochemical synthesis of hydroxyapatite using cuttlefish bone and chicken eggshell as calcium precursors. *Mater. Sci. Eng. C* **2019**, *97*, 124–140. [CrossRef]
36. Ferro, A.C.; Seixas, T.; Guedes, M. Reaction path in the mechanosynthesis of calcium phosphates using a biogenic calcium source. *Ceram. Int.* **2024**, *50*, 282–292. [CrossRef]
37. Suryanarayana, C. Mechanical alloying and milling. *Prog. Mater. Sci.* **2001**, *46*, 1–184. [CrossRef]
38. Baláž, P.; Achimovičová, M.; Baláž, M.; Billik, P.; Cherkezova-Zheleva, Z.; Criado, J.M.; Delogu, F.; Dutková, E.; Gaffet, E.; Gotor, F.J.; et al. Hallmarks of mechanochemistry: From nanoparticles to technology. *Chem. Soc. Rev.* **2013**, *42*, 7571. [CrossRef]
39. Pham Minh, D.; Lyczko, N.; Sebei, H.; Nzihou, A.; Sharrock, P. Synthesis of calcium hydroxyapatite from calcium carbonate and different orthophosphate sources: A comparative study. *Mater. Sci. Eng. B* **2012**, *177*, 1080–1089. [CrossRef]

40. Wu, S.C.; Hsu, H.C.; Hsu, S.K.; Chang, Y.C.; Ho, W.F. Effects of heat treatment on the synthesis of hydroxyapatite from eggshell powders. *Ceram. Int.* **2015**, *41*, 10718–10724. [CrossRef]
41. Brown, P.W.; Hocker, N.; Hoyle, S. Variations in Solution Chemistry During the Low-Temperature Formation of Hydroxyapatite. *J. Am. Ceram. Soc.* **1991**, *74*, 1848–1854. [CrossRef]
42. Peng, S.Y.; Lin, Y.W.; Lin, Y.Y.; Lin, K.L. Hydrothermal synthesis of hydroxyapatite nanocrystals from calcium-rich limestone sludge waste: Preparation, characterization, and application for Pb^{2+} adsorption in aqueous solution. *Inorg. Chem. Commun.* **2024**, *160*, 111943. [CrossRef]
43. Akram, M.; Ahmed, R.; Shakir, I.; Ibrahim, W.A.W.; Hussain, R. Extracting hydroxyapatite and its precursors from natural resources. *J. Mater. Sci.* **2014**, *49*, 1461–1475. [CrossRef]
44. European Commission. LIFE Project. (2011–2014). Sludges from Agglomerated Stones Industry for Environmental Sustainability (LIFE10 ENV/IT/000346). 2025. Available online: https://webgate.ec.europa.eu/life/publicWebsite/project/LIFE10-ENV-IT-000346 (accessed on 28 September 2025).
45. Arif, S. Synthesis of Biomaterial Hydroxyapatite from Limestone by Using Two-Step Conversion. *Int. J. Sci. Eng. Inf. Technol.* **2020**, *5*, 236–238. [CrossRef]
46. El-Mehalawy, N.; Sayed, M.; Abou El-Anwar, E.A.; Soliman, A.A.F.; Naga, S.M. Preparation and characterization of bioceramic composites based on anorthite and β-TCP from dolomitic phosphate and kaolin rocks. *Mater. Chem. Phys.* **2024**, *312*, 128625. [CrossRef]
47. Vu, H.H.T.; Khan, M.D.; Chilakala, R.; Lai, T.Q.; Thenepalli, T.; Ahn, J.W.; Park, D.U.; Kim, J. Utilization of Lime Mud Waste from Paper Mills for Efficient Phosphorus Removal. *Sustainability* **2019**, *11*, 1524. [CrossRef]
48. Yatongchai, C.; Thavornyutikarn, B. Conversion of lime mud waste to hydroxyapatite biomaterials. *Mater. Chem. Phys.* **2021**, *266*, 124544. [CrossRef]
49. *ISO 638:2008*; Paper, Board and Pulps—Determination of Dry Matter Content—Oven Drying Method. ISO: Geneva, Switzerland, 2008.
50. Wojdyr, M. Fityk: A general-purpose peak fitting program. *J. Appl. Crystallogr.* **2010**, *43*, 1126–1128. [CrossRef]
51. Schneider, C.A.; Rasband, W.S.; Eliceiri, K.W. NIH Image to ImageJ: 25 years of image analysis. *Nat. Methods* **2012**, *9*, 671–675. [CrossRef]
52. Bruker. X-ray Powder Diffraction in Pharma—Amorphous Content Determination and Degree of Crystallinity. *Appl. Rep. XRD* **2017**, *36*, 1–2.
53. Doebelin, N.; Kleeberg, R. Profex: A graphical user interface for the Rietveld refinement program BGMN. *J. Appl. Crystallogr.* **2015**, *48*, 1573–1580. [CrossRef]
54. Toby, B.H. R factors in Rietveld analysis: How good is good enough? *Powder Diffractom.* **2006**, *21*, 67–70. [CrossRef]
55. Yılmaz, Ö.; Yontem, E.; Ozdogru, Z. D1.3 Inventory of Raw Materials, Waste, and Energy Flows in Industrial Sectors—Summary Report. FISSAC Project, EKODENGE. 2018. Available online: https://fissacproject.eu/wp-content/uploads/2018/06/FISSAC-D1.3-Inventory-of-raw-materials-waste-and-energy-flows-in-industrial-sectors-Summary.pdf (accessed on 28 September 2025).
56. Lewis, J.A. Colloidal Processing of Ceramics. *J. Am. Ceram. Soc.* **2000**, *83*, 2341–2359. [CrossRef]
57. Kitanaka, R.; Tsuboi, M.; Ozaki, Y. Biogenic apatite in carbonate concretions with and without fossils investigated in situ by micro-Raman spectroscopy. *Sci. Rep.* **2023**, *13*, 9714. [CrossRef]
58. Rey, C.; Combes, C.; Drouet, C.; Grossin, D. Bioactive Ceramics: Physical Chemistry. In *Comprehensive Biomaterials*; Ducheyne, P., Healy, H.E., Hutmacher, D.W., Grainger, D., kirkpatrcik, C.J., Eds.; Elsevier: Amsterdam, The Netherlands, 2011; pp. 187–221. [CrossRef]
59. Rudolph, W.W. Raman- and infrared-spectroscopic investigations of dilute aqueous phosphoric acid solutions. *Dalton Trans.* **2010**, *39*, 9642. [CrossRef]
60. Fleet, M.E.; Liu, X.; King, P.L. Accommodation of the carbonate ion in apatite: An FTIR and X-ray structure study of crystals synthesized at 2–4 GPa. *Am. Mineral.* **2004**, *89*, 1422–1432. [CrossRef]
61. Paquette, J.; Reeder, R.J. Single-crystal X-ray structure refinements of two biogenic magnesian calcite crystals. *Am. Mineral.* **1990**, *75*, 1151–1158.
62. Macphee, D.E.; Lachowski, E.E. Cement Components and Their Phase Relations. In *Lea's Chemistry of Cement and Concrete*; Hewlett, P.C., Ed.; Elsevier: Amsterdam, The Netherlands, 1998; pp. 95–129. [CrossRef]
63. Gabbott, P. Fast Scanning DSC. In *Principles and Applications of Thermal Analysis*; Wiley: Hoboken, NJ, USA, 2008; pp. 51–86. [CrossRef]
64. Allen, T. *Particle Size Measurement*, 2nd ed.; Chapman and Hall: London, UK, 1975. [CrossRef]
65. Toshima, T.; Hamai, R.; Tafu, M.; Takemura, Y.; Fujita, S.; Chohji, T.; Tanda, S.; Li, S.; Qin, G.W. Morphology control of brushite prepared by aqueous solution synthesis. *J. Asian Ceram. Soc.* **2014**, *2*, 52–56. [CrossRef]
66. Lago-Vila, M.; Rodríguez-Seijo, A.; Arenas-Lago, D.; Andrade, L.; Vega, M.F.A. Heavy metal content and toxicity of mine and quarry soils. *J. Soils Sediments* **2017**, *17*, 1331–1348. [CrossRef]

67. *ISO 13175-3:2012(E)*; Implants for Surgery—Calcium Phosphates—Part 3: Hydroxyapatite and Beta-Tricalcium Phosphate Bone Substitutes (13175-3). ISO: Geneva, Switzerland, 2012.
68. Thomas, D.B.; McGoverin, C.M.; Fordyce, R.E.; Frew, R.D.; Gordon, K.C. Raman spectroscopy of fossil bioapatite—A proxy for diagenetic alteration of the oxygen isotope composition. *Palaeogeogr. Palaeoclimatol. Palaeoecol.* **2011**, *310*, 62–70. [CrossRef]
69. Burany, S. *Scanning Electron Microscopy and X-Ray Microanalysis*. J. Goldstein, D. Newbury, D. Joy, C, Lyman, P. Echlin, E. Lifshin, L. Sawyer, and J. Michael. Kluwer Academic, Plenum Publishers, New York. *Microsc. Microanal.* **2003**, *9*, 484. [CrossRef]
70. Ho, W.F.; Hsu, H.C.; Hsu, S.K.; Hung, C.W.; Wu, S.C. Calcium phosphate bioceramics synthesized from eggshell powders through a solid state reaction. *Ceram. Int.* **2013**, *39*, 6467–6473. [CrossRef]
71. Gomes, D.S.; Santos, A.M.C.; Neves, G.A.; Menezes, R.R. A brief review on hydroxyapatite production and use in biomedicine. *Cerâmica* **2019**, *65*, 282–302. [CrossRef]
72. Wang, L.; Nancollas, G.H. Calcium Orthophosphates: Crystallization and Dissolution. *Chem. Rev.* **2008**, *108*, 4628–4669. [CrossRef]
73. Andersen, C.B. Understanding Carbonate Equilibria by Measuring Alkalinity in Experimental and Natural Systems. *J. Geosci. Educ.* **2002**, *50*, 389–403. [CrossRef]
74. Francis, M.D.; Webb, N.C. Hydroxyapatite formation from a hydrated calcium monohydrogen phosphate precursor. *Calcif. Tissue Res.* **1970**, *6*, 335–342. [CrossRef]
75. de Groot, K. Effect of Porosity and Physicochemical Properties on the Stability, Resorption, and Strength of Calcium Phosphate Ceramics. *Ann. N. Y. Acad. Sci.* **1988**, *523*, 227–233. [CrossRef] [PubMed]